Characterizing the carrier-envelope phase stability of mid-infrared laser pulses by high harmonic generation in solids

A. Leblanc, P. Lassonde, Gilles Dalla-Barba, E. Cormier, H. Ibrahim, F. Légaré

Characterizing the carrier-envelope phase stability of mid-infrared laser pulses by high harmonic generation in solids

A. LEBLANC,[1,2] P. LASSONDE,[1] GILLES DALLA-BARBA,[3] E. CORMIER, [3,4] H. IBRAHIM, [1] AND F. LÉGARÉ, [1*]

[1] *Institut National de la Recherche Scientifique, Centre EMT, ALLS laboratory, 1650 Boulevard Lionel-Boulet, Varennes, Qc, J3X1S2, Canada*
[2] *Laboratoire d'Optique Appliquée, Ecole Polytechnique, ENSTA, CNRS, Université Paris Saclay, Palaiseau, France*
[3] *Laboratoire Photonique Numérique et Nanosciences (LP2N), UMR 5298, CNRS-IOGS-Université Bordeaux, 33400 Talence, France*
[4] *Institut Universitaire de France (IUF),1 rue Descartes, 75231 Paris, France*
[*] *legare@emt.inrs.ca*

Abstract: We present a novel approach for measuring the carrier-envelope phase (CEP) stability of a laser source by employing the process of high harmonic generation (HHG) in solids. HHG in solids driven by few-cycle pulses is very sensitive to the waveform of the driving pulse, therefore enabling to track the shot-to-shot CEP fluctuations of a laser source. This strategy is particularly practical for pulses at long central wavelength up to the mid-infrared spectral range where usual techniques used in the visible or near-infrared regions are challenging to transpose. We experimentally demonstrate this novel tool by measuring the CEP fluctuations of a mid-infrared laser source centered at 9.5 μm.

1. Introduction

Today's commercial laser technologies routinely provide laser pulses with durations of a few tens of femtoseconds, with the most advanced laser sources delivering pulses down to the single-cycle limit [1]. In this regime, the waveform of the electromagnetic field under the pulse envelope varies with the carrier-envelope phase, and plays a key role in the outcome of nonlinear interactions with atoms [2–4], molecules [5–7], and solids [8–11]. In particular, control of the CEP was the key technological milestone to generate isolated attosecond pulses [12–14].

Nearly two decades ago, various techniques were explored to track and control the CEP of mode-locked oscillators [15–17] with the demonstration of controlling the phase evolution of few-cycle light pulses from oscillators to seed kHz chirped pulse amplification laser systems [18]. Based on this pioneering work, most techniques used nowadays to measure the CEP stability of laser sources are based on the interferometry of two pulses, derived from the initial pulse to be characterized. This pulse is divided into two arms: one to be up-converted to the second [19–21] or third [22, 23] harmonic of the fundamental frequency, and the second one to be spectrally broadened by supercontinuum generation until its spectrum overlaps with the harmonic of the first arm. In this particular spectral range, interference between the two arms results in fringes following the CEP of the fundamental pulse. Indeed, while the spectral distance of the fringes is determined by the fixed delay between the two arms, their position directly depends on the CEP. Therefore, the observation and single-shot measurement of the position of these fringes enables to (**i**) demonstrate the capability to stabilize and control the CEP for a specific architecture or design of a laser source; (**ii**) measure the shot-to-shot fluctuations of the CEP and evaluate the CEP stability by recording these fluctuations over many single-shot measurements; (**iii**) implement a

loop to retro-actively correct for the long-term drifts of the CEP.

While for many applications only the relative phase variation from shot-to-shot is sufficient to be known, other techniques enable to characterize the absolute phase of a laser field [24], such as stereo-ATI [2] (above threshold ionization) or electro-optical sampling [25, 26], but they are in general more complex to implement than techniques that only measure the relative CEP variations.

Recently, the generation of octave (and beyond) spanning spectra and CEP stabilized femtosecond pulses at long wavelengths towards the mid-IR spectral range has become a very active field driven by a wide variety of applications, at both low repetition rate for high energy pulses [20, 26–28] and high repetition rate for high average power [29–32]. For example, such high energy mid-infrared (IR) pulses are promising to extend the generation of attosecond pulses towards the soft X-rays through HHG in gas [33–35]; to provide new tools for studying condensed matter physics such as HHG in solids [36, 37] and for the sub-cycle control of electronic dynamics in low bandgap materials [38]; as well as to perform photoelectron streaking with a combined large temporal window and a high temporal resolution [39].

However, there is still a lack of practical diagnostics to measure the CEP stability of such pulses. Therefore, recent works [27, 30] presenting novel schemes to generate CEP stable mid-IR pulses assume the stability of their waveform because the source is based on difference frequency generation (DFG) between phase-locked frequencies, an approach that was proven to provide CEP stable pulses in the near-IR [40]. But these studies contain no measurement to properly show the CEP stability because, to date, it is very challenging to transpose the metrologies available to measure the CEP stability in the near-IR and IR to the mid-IR. In fact, very few (and very expensive) spectrometers enable single-shot measurements above 2.5 μm, thus, f-2f and f-3f interferometry techniques cannot be implemented easily above 5 and 7.5 μm respectively. Liang and co-workers [41] proposed the f-3f approach to measure the CEP stability of a mid-IR source centered at 6.4 μm. Using DFG between near-IR and mid-IR pulses and the interference with a replica of the near-IR pulse, single-shot tracking of the CEP of mid-IR pulses centered at 17 μm was realized [42].

While using the f-2f and f-3f approaches for the mid-IR spectral range are currently limited by the range of available detectors, we are exploring an alternative strategy. Recent publications [43–45], focusing on the understanding of the HHG mechanisms by comparing theoretical models to the experimental results, have shown that HHG in solids driven by few-cycle pulses is highly sensitive to the CEP, confirming to some extent the CEP stability of the source. A drift in the shape of the harmonic spectra and position of its peaks is observed while tuning the CEP.

In the present paper, we propose to use this process as a novel class of diagnostics to track and measure the CEP stability of a laser source. As the position of the harmonic peaks encodes the CEP of the driving pulse, we perform a first measurement to record the harmonic spectrogram as a function of the CEP, averaged over many shots to smooth the effect of remaining CEP fluctuations. Note that acquiring such spectrogram already demonstrates the CEP stability of the source and the capability to control the laser waveform. In addition, single-shot measurements of the harmonic spectra are taken, and their spectral profiles are compared to the reference spectrogram for the extraction of the relative CEP for every shot. Finally, single-shot measurements over many laser shots enable to evaluate the CEP fluctuations of the source. Note that the proposed phase meter is only sensitive to the relative phase variations from shot-to-shot which provides sufficient information for many applications.

This characterization method simplifies drastically the experimental setup compared to interferometry, given that the source has sufficient peak power to drive high harmonic generation from solids. Note that there has been recent progresses for driving HHG from solids with high repetition rate IR laser systems delivering $\sim$10 nanojoules pulses through the enhancement of the process with nanostructures [46]. Combined with our approach, this could be useful to

characterize the CEP fluctuations of high repetition rate mid-IR laser sources. As based on HHG in solids, the signal to measure in the proposed technique is transposed to high orders of the fundamental wavelength. Thus, it is naturally suited for the characterization of the relative CEP of pulses in the mid-IR range since HHG in solids can easily reach wavelengths towards the near-IR and the visible where ultra-sensitive spectrometers are widely available for single-shot measurements. Here, this approach is demonstrated experimentally by measuring the CEP stability of a source that delivers mid-IR pulses centered at 9.5 μm.

2. Experimental results for the HHG in a solid

The experiments were performed at the Advanced Laser Light Source facility located at INRS-EMT. To generate the mid-IR pulses, we use a chirped pulse amplification (CPA) Ti-Sa laser system that delivers femtosecond pulses at a repetition rate of 100 Hz with the central wavelength at 800 nm. The architecture to derive CEP stable mid-IR pulses is based on combining the strengths of two approaches developed at ALLS. First, using Frequency domain Optical Parametric Amplification (FOPA) [47], two spectral slices of broadband 1.8 μm pulses are amplified in the Fourier plane. Second, the relative delay and polarization of these two spectral slices are controlled using a window and a half waveplate installed in the Fourier plane of the FOPA for shaping the pulses [48]. At the output of the FOPA, intrapulse DFG is performed between two spectral slices, centered respectively at 1.7 and 1.95 μm, in a z-cut gallium selenide (GaSe) crystal whose thickness is 750 μm. Finally, a long pass filter (LP6715, Spectrogon) selects only the spectral components above 6.7 μm. Using this approach, we have recently demonstrated the generation of high-field CEP stable mid-IR pulses centered at 9.5 μm with a duration of two cycles and an energy of 25.5 μJ (±3.5% rms, obtained from statistics of single-shot pulse energy measurements) [28].

In most studies where CEP stable mid-IR pulses are generated, the intrapulse DFG mechanism is involved [27, 30]. It was demonstrated to provide passively stabilized CEP in the near-IR [40]. With this strategy, the absolute CEP depends on the relative delay between the two spectral slices involved in the DFG process. Here, in the FOPA setup, we control this delay with the rotation of a compensating window placed in the optical path of one spectral slice of the broadband pulses (see ref. [28, 48]), thus providing a direct control of the waveform of the mid-IR pulses.

In this work, the mid-IR waveform is tuned by varying the delay between the two spectral slices that drive the DFG process [28]. In the FOPA setup, the polarization of the 1.95 μm spectral slice is rotated by a half wave plate. The relative delay of the 1.7 μm spectral slice is compensated by a fused silica window whose thickness is $d_2 = 2$ mm and optical index is $n_2 = 1.4422$ at $\lambda_2 = 1.7$ μm. It is placed on an accurate rotation stage (CR1-Z7, Thorlabs) at an incident angle of θ. The relative phase between the two spectral slices is therefore given by the following expression:

$$\Delta\phi = \frac{2\pi}{\lambda_2} \cdot d_2 \left[n_2 \cos\left(\arcsin(\sin\theta/n_2) \right) - \cos\theta \right] - \frac{2\pi}{\lambda_1} \cdot n_1 d_1 \tag{1}$$

with d_1 and n_1 the thickness and optical index of the half wave plate at $\lambda_1 = 1.95\mu$m. At $\Delta\phi = 0$, for an incident angle of approximately $\theta_0 \sim 12°$, the DFG process is optimized and the mid-IR pulses energy is maximized. A change in the relative delay translates in a phase shift between the two spectral slices driving the DFG. From the optimized position θ_0, the relative CEP of the mid-IR pulses is tuned by slight rotations and can be directly calculated by the phase shift $\Delta\phi(\theta) - \Delta\phi(\theta_0)$ between the two spectral slices with the expression:

$$\text{relative CEP} = \frac{2\pi d_2}{\lambda_2} \cdot \left[\left[n_2 \cos\left(\arcsin(\sin\theta/n_2) \right) - \cos\theta \right] - \left[n_2 \cos\left(\arcsin(\sin\theta_0/n_2) \right) - \cos\theta_0 \right] \right] \tag{2}$$

From this calculation, we deduce that tuning θ from $\sim 9°$ to $\sim 13.5°$ enables to scan over six optical cycles the relative CEP of the mid-IR pulses. Note that this result is verified experimentally (as observed further in Fig. 2).

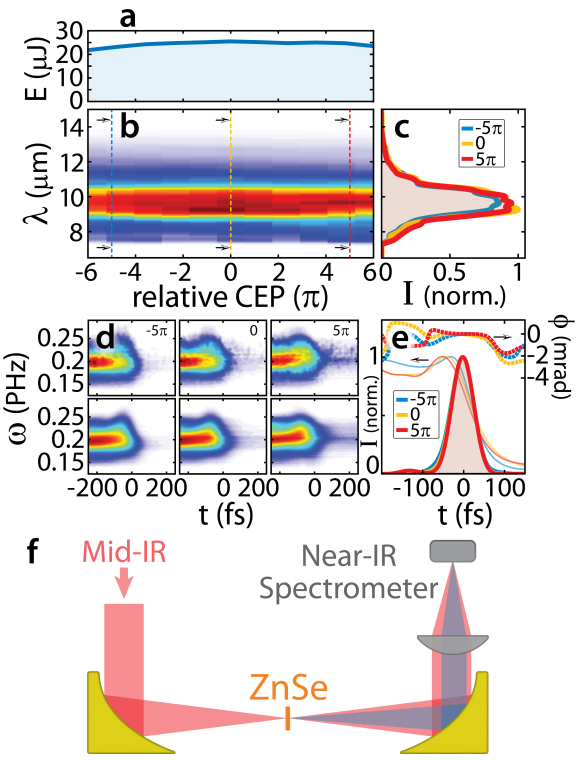

Fig. 1. Mid-IR pulse energy, panel **a**, and spectra, panels **b** and **c**, for different positions of the relative CEP (Eq. 2 normalized by π). – **d** – Experimental (top panels) and reconstructed (lower panels) FROSt spectrograms for three different relative CEP positions of -5π, 0, and 5π. – **e** – Retrieved temporal profiles of the mid-IR pulses in intensity, full thick lines, and phase, dash lines, and of the optical switch (see [49]) in intensity, full light lines. – **f** – Experimental setup for the generation and detection of high harmonics generated in a zinc selenide window (two off-axis parabolic mirrors of 50 mm focal length, and a 100 mm lens).

Different properties of the mid-IR laser source are presented in Fig. 1. The energy per pulse in panel **a** and spectra in panels **b** and **c** are presented as a function of the relative CEP of the mid-IR pulses normalized by π. The spectrometer is based on the CM110 monochromator from Spectral Products, with the HgCdTe (HCT) bolometric detector from Infrared Associates Inc. cooled with liquid nitrogen. In addition, as presented in panels **d** and **e**, the mid-IR pulses are measured temporally for three different relative CEP of -5π, 0, and 5π with the frequency-resolved optical switching (FROSt) technique [49]. To perform this FROSt measurement, a few- μJ of energy of the mid-IR beam is focused with a 5mm off-axis parabola onto a 300 μm thick germanium (Ge) plate. In parallel, the 1.95 μm beam reflected by the long pass filter after the DFG is frequency doubled to ~1 μm by a 2 mm thick type-I BBO crystal. These ~120 μJ pulses are used to pump the Ge plate to create an optical switch for the FROSt measurements. The transmitted mid-IR spectra through the Ge plate are measured as a function of the relative delay with the 1 μm pulses. The experimental and reconstructed (with a phase retrieval algorithm, see ref. [49]) spectrograms for the three relative CEP are shown in Fig. 1**d**. Finally, the temporal intensity and phase profiles are presented in panel **e**. The full width at half maximum (FWHM) duration in intensity of the

mid-IR pulses are respectively measured to 67, 66 and 64 fs for relative CEP of -5π, 0, and 5π.

The experimental setup used to characterize the CEP stability is illustrated in Fig. 1**b**. The mid-IR pulses are directly focused in a solid for HHG, here a zinc selenide (ZnSe) window of 500 μm thickness. Then, the harmonic beam is collected in a spectrometer. Here, the mid-IR field strength at the sample is estimated to ~45MV/cm. Figure 2 shows the harmonic spectrogram measured in the ~1 to 2.5 μm spectral range (corresponding to harmonic orders from ~ 4^{th} to 10^{th}) with a near-IR spectrometer (NIR256-2.5, Ocean Optics) as a function of the relative CEP of the driving pulse. Each spectra results from the average of 200 laser shots (2s). As previously observed [43–45], the harmonic spectra significantly vary with the CEP with a drift in wavelength of the harmonic peaks. Similarly to the half-cycle cut-off from gas phase HHG [50], we observe that the extension of the HHG spectra from ZnSe depends on the CEP.

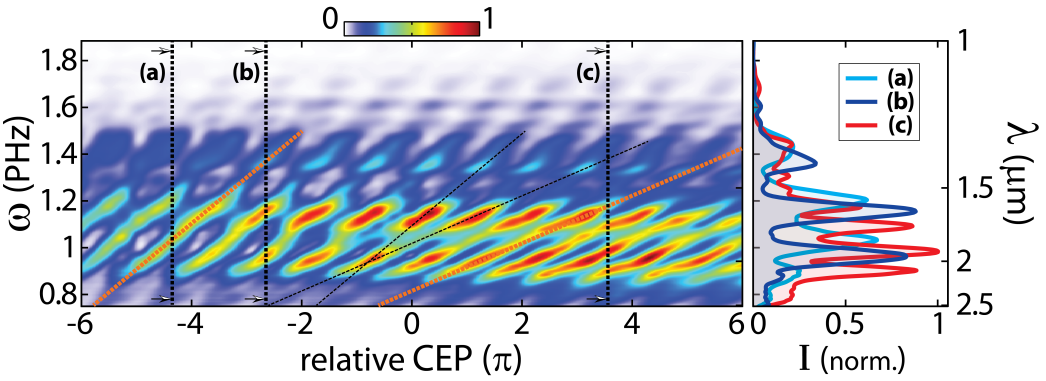

Fig. 2. Harmonic spectra measured in intensity as a function of the relative CEP of the mid-IR pulses (Eq. 2 normalized by π). Oblique lines highlight the drift in wavelength of the harmonic peaks. The positions of the following three measurements of the CEP fluctuations at a fixed CEP of -4.34π, -2.64π and 3.56π are respectively represented with the vertical lines **(a)**, **(b)**, and **(c)**. The harmonic profile at these three positions is shown on the right panel.

Changing the relative phase (and delay) between the two spectral slices (see Eq. 1) not only tune the CEP of the mid-IR pulses but also slightly changes the energy of the mid-IR pulses. For instance, for a relative CEP position of -6π, the energy decreases to ~22 μJ, see Fig. 1**a**. This explains also why the harmonic signal is lower at this relative CEP. Moreover, as can be observed in the panels **b**, **c**, and **e** of Fig. 1, the pulse spectra and duration are very similar when varying the relative CEP from -6π to +6π. We can conclude from all these measurements that the periodic variation of the harmonic spectra observed in Fig. 2 mainly results from the change of the CEP of the mid-IR pulses and not from variations of their energy, spectra, or duration. Note that these slight changes in the generation of the mid-IR pulses (energy, spectra, duration) do not affect the CEP stability of the source that is determined by the stability of the FOPA setup (e.g. mechanical vibrations, turbulences, etc).

In our experiment, we observe two different HHG regimes. As shown in the right panel of Fig. 2 (compare for instance the harmonic profiles **(b)** and **(c)**), for CEP > 2π there are twice as many harmonic peaks as for CEP < -2π. The oblique dash lines in orange in the left panel highlight that in these two regimes, the harmonic peaks drift approximately linearly with the CEP variation as previously observed in different publications [43–45]. The slopes of these drifts with the relative CEP are different because the HHG spectrum shape changes, with twice as many harmonic peaks above a relative CEP of 2π compared to below -2π. Note that even with this change in the slopes, the period at which the HHG varies with the relative CEP remains π. The

two oblique lines are copied at a CEP = 0 as a thin dash line in black to highlight the transition between the two regimes. To date, we do not understand this change in the HHG spectra, however explaining this observation is related to the nature the HHG process itself and its explanation is out of the scope of this study that focuses on the measurement of the relative CEP of the mid-IR source and its fluctuations.

3. Experimental measurement of the CEP stability

While the measurement presented in Fig. 2 demonstrates the CEP stability of the source, it does not characterize its shot-to-shot fluctuations. For this evaluation, we perform single-shot measurements of the harmonic spectrum for a fixed angle θ of the compensating window in the 4f-setup and we compare the single-shot spectrum with the reference spectrogram. To demonstrate the validity of this evaluation, this measurement is performed at three different fixed relative CEP positions over the two regimes where the harmonic peaks drift linearly with the CEP. These positions are identified in Fig. 2 by the vertical dashed lines in black **(a)**, **(b)**, and **(c)** (respective CEP positions of -4.34π, -2.64π and 3.56π). These single-shot measurements of the harmonic spectrum over more than 8000 shots (80s at 100Hz) at these three different positions are respectively shown in the top panels of Fig. 3**a**, **b** and **c**.

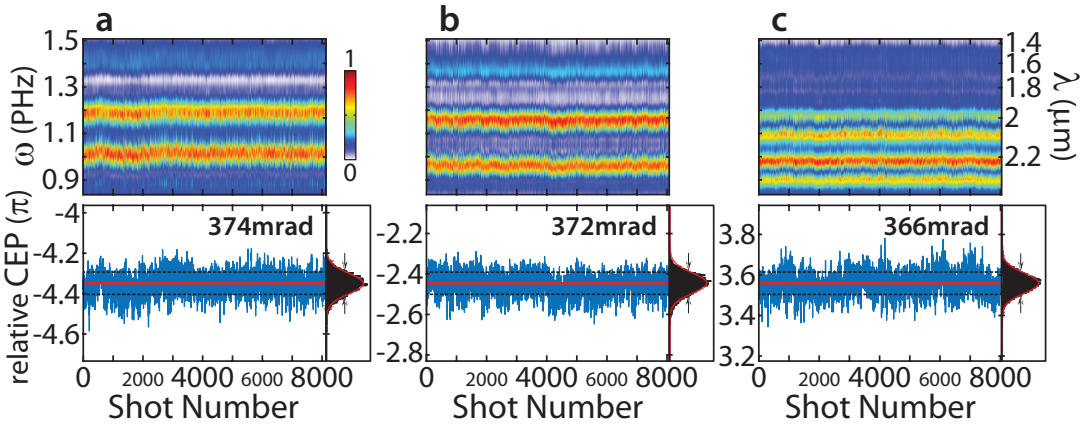

Fig. 3. Single-shot measurements over more than 8000 shots for a fixed relative CEP position (the compensating window angle is fixed in the source architecture) of -4.34π for panels **a**, -2.64π for panels **b**, and 3.56π for panels **c**, respectively corresponding to vertical line **(a)**, **(b)**, and **(c)** in Fig. 2. – Intensity spectra are presented in the top panels. – In the lower panels is presented the relative CEP of each shot extracted from the comparison of each single-shot spectrum to the reference spectrogram by the procedure illustrated in Fig. 4. The histogram of the relative CEP distribution are shown at the right of each panel.

The harmonic drift with the CEP variation is only approximately linear in the two regimes due to the wide transition between both. For instance in Fig. 2, at a relative CEP position of -2π, close to the measurement **(b)**, the drift of the most intense HHG peak is not exactly linear as already located in the transition. This complexity in the HHG process does not allow to directly deduce the relative CEP of one shot from the position of the harmonic peaks. Therefore, the Fourier analysis procedures used to extract the relative CEP from the interference pattern obtained by f-2f measurements, where the fringes directly map the relative CEP with a linear drift, cannot be used here.

To extract the relative CEP in single-shot, we compare its harmonic spectrum to each spectra of the reference spectrogram (see Fig. 2). This comparison is illustrated in Fig. 4, for the first shots of each three measurements presented in Fig. 3. For a CEP window around the expected relative

CEP position, here $\pm 0.4\pi$, the single-shot harmonic profile $I_{\text{single-shot}}(\omega)$, top right panels in Fig. 4, is compared to each profile of the spectrogram $I_{\text{average}}(\omega, \text{CEP})$, top left panels in Fig.4. The difference of the single-shot profile to the spectrogram ones is evaluated by the following expression:

$$\varepsilon(\text{CEP}) = \sqrt{1 - \frac{|\int I_{\text{single-shot}}(\omega) \cdot I_{\text{average}}(\omega, \text{CEP})\, d\omega|^2}{\int |I_{\text{single-shot}}(\omega)|^2 d\omega \cdot \int |I_{\text{average}}(\omega, \text{CEP})|^2 d\omega}} \tag{3}$$

The difference $\varepsilon(\text{CEP})$ is plotted as a function of the relative CEP in the lowest panels on Fig. 4. The relative CEP of the considered single shot is determined by the minimum of $\varepsilon(\text{CEP})$. Note that instead of considering which profile in the spectrogram $I_{\text{average}}(\omega, \text{CEP})$ is the closest to the single-shot one, the accuracy of the measurement is improved by a parabolic fitting of $\varepsilon(\text{CEP})$ around its minimum value (see sub-panels on Fig. 4). This parabolic fitting is only an analysis tool to evaluate the relative CEP with a higher accuracy than the measurement CEP step.

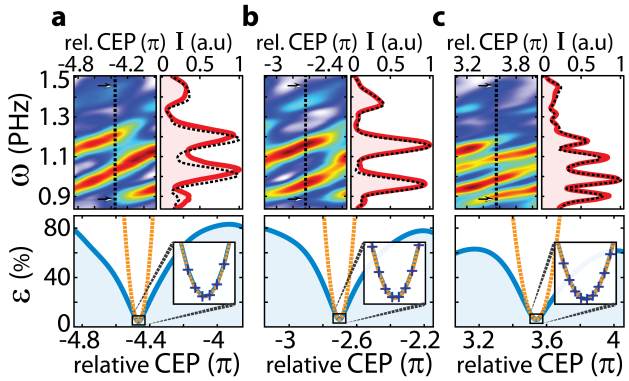

Fig. 4. Example of the extraction of the relative CEP position of a single-shot for the first 3 shots of each measurement presented in the top panels of Fig. 3**a**, **b**, and **c**. – Top left panel: zoom in ($\pm 0.4\pi$) around the average position of -4.34π, -2.64π, and 3.56π in panels **a**, **b**, and **c**, of the harmonic spectrogram $I_{\text{average}}(\omega, \text{CEP})$ illustrated in Fig. 2. – Top right panel: harmonic profile in intensity of the first single-shot measurement, $I_{\text{single-shot}}(\omega)$, presented in the top panels of Fig. 3 in solid red line, and the profile of the spectrogram corresponding to the relative CEP positions of -4.34π, -2.64π and 3.56π in dashed black line (relative CEP position illustrated by the vertical dash line in the left panel). – Bottom panel: difference $\varepsilon(\text{CEP})$ in percentage between the single-shot harmonic profile and the spectrogram profiles as a function of the CEP calculated by Eq. 3. The sub-panel shows how the accurate single-shot relative CEP position is determined by the position of a parabolic fitting around the minimum of $\varepsilon(\text{CEP})$.

This procedure to evaluate the relative CEP is performed for each single-shot spectrum, and the deduced relative CEP as a function of the shot number is illustrated in the lower panels of Fig. 3. Finally, the CEP fluctuation is evaluated by the full width at half maximum of the Gaussian fit of the histogram of the relative CEP distribution for all shots (see Fig. 3). At the relative CEP positions -4.34π **(a)**, -2.64π **(b)**, and 3.56π **(c)** (see Fig. 2) the CEP stability is measured respectively to 374, 372, and 366 mrad, thus the CEP fluctuations of the source are evaluated to 371 ± 4 mrad. While these three measurements are independent, performed over more than 24000 shots, and located in two different regimes of the harmonic drift with the CEP, they provide results that are very similar. These results demonstrate the reliability of this procedure.

Note that this evaluation represents only an estimation of the upper limit of the CEP fluctuations. On top of the CEP fluctuations of the source due to the stability of the whole setup, there are

also energy fluctuations from shot-to-shot (evaluated to ±3.5%) that can slightly affect the HHG process on which the proposed measurement is based. The addition of these two effects result in an artificial increase of the measured CEP fluctuations compared to the effective CEP fluctuations. This effect is also observed for f-2f (or f-3f) measurements [51, 52].

4. Conclusion

In this paper, we introduce a novel technique to demonstrate and measure the CEP stability of a laser source delivering few-cycle pulses. By using the dependency of HHG in solids with the CEP of the driving pulse, and comparing a single-shot harmonic spectrum to the HHG spectrogram (HHG spectra vs CEP), we have shown that the relative CEP can be measured in single shot, thus our method is sensitive to shot-to-shot fluctuations. To the best of our knowledge, this is the first time HHG in solids is used to measure the CEP fluctuations of a laser source.

This technique is particularly useful to characterize the CEP stability of pulses centered at long wavelengths towards the mid-IR, as to date no simple tool enables such measurement in this spectral range. The method presented here is very easy to implement and can be easily transferred to other laser wavelength as pulses with sufficient field strengths to generate harmonics in solids are available from the NIR to the THz spectral range [36].

This tool can be used for active correction of the CEP drift of a laser source. However, the accurate CEP characterization presented in Fig. 4 may be slow due to the time required to compare a single-shot spectrum with multiple spectra contained in the reference spectrogram. This data treatment can be made faster by only considering the position of the maximum of one harmonic peak. While less accurate, this strategy provides an upper limit of the CEP fluctuations thus enabling rapid feedback for the purpose of active correction.

Ackowledgements

A. Leblanc acknowledges funding from the European Union's Horizon 2020 research and innovation programme under the Marie Skłodowska-Curie Grant Agreement No. 798205, and from the Canadian Banting Research Foundation No. 201709BPF-393834-285459. E. Cormier acknowledges funding from the Institut Universitaire de France.

Disclosures

The authors declare no conflicts of interest.

References

1. A. Wirth, M. T. Hassan, I. Grguraš, J. Gagnon, A. Moulet, T. T. Luu, S. Pabst, R. Santra, Z. Alahmed, A. Azzeer, V. S. Yakovlev, V. Pervak, F. Krausz, and E. Goulielmakis, "Synthesized light transients," *Science* **334**, 195–200 (2011).
2. G. G. Paulus, F. Lindner, H. Walther, A. Baltuška, E. Goulielmakis, M. Lezius, and F. Krausz, "Measurement of the phase of few-cycle laser pulses," *Phys. review letters* **91**, 253004 (2003).
3. F. Lindner, M. G. Schätzel, H. Walther, A. Baltuška, E. Goulielmakis, F. Krausz, D. Milošević, D. Bauer, W. Becker, and G. G. Paulus, "Attosecond double-slit experiment," *Phys. review letters* **95**, 040401 (2005).
4. E. Goulielmakis, Z.-H. Loh, A. Wirth, R. Santra, N. Rohringer, V. S. Yakovlev, S. Zherebtsov, T. Pfeifer, A. M. Azzeer, M. F. Kling, S. R. Leone, and F. Krausz, "Real-time observation of valence electron motion," *Nature* **466**, 739 (2010).
5. M. Kling, C. Siedschlag, A. J. Verhoef, J. Khan, M. Schultze, T. Uphues, Y. Ni, M. Uiberacker, M. Drescher, F. Krausz, and M. J. J. Vrakking, "Control of electron localization in molecular dissociation," *Science* **312**, 246–248 (2006).
6. G. Sansone, F. Kelkensberg, J. Pérez-Torres, F. Morales, M. F. Kling, W. Siu, O. Ghafur, P. Johnsson, M. Swoboda, E. Benedetti, F. Ferrari, F. Lépine, J. L. Sanz-Vicario, S. Zherebtsov, I. Znakovskaya, A. L'Huillier, M. Y. Ivanov, M. Nisoli, F. Martin, and M. J. J. Vrakking, "Electron localization following attosecond molecular photoionization," *Nature* **465**, 763 (2010).
7. H. Li, B. Mignolet, G. Wachter, S. Skruszewicz, S. Zherebtsov, F. Shussmann, A. Kessel, A. Trushin, Sergei, N. G. Kling, M. Kübel, B. Ahn, D. Kim, I. Ben-Itzhak, C.-L. Cocke, T. Fennel, J. Tiggesbaumker, K.-H. Meiwes-Broer, C. Lemell, J. Burgdorfer, R.-D. Levine, F. Remacle, and M.-F. Kling, "Coherent electronic wave packet motion in c 60 controlled by the waveform and polarization of few-cycle laser fields," *Phys. review letters* **114**, 123004 (2015).

8. M. Krüger, M. Schenk, and P. Hommelhoff, "Attosecond control of electrons emitted from a nanoscale metal tip," *Nature* **475**, 78 (2011).
9. A. Schiffrin, T. Paasch-Colberg, N. Karpowicz, V. Apalkov, D. Gerster, S. Mühlbrandt, M. Korbman, J. Reichert, M. Schultze, S. Holzner, J. V. Barth, R. Kienberger, R. Ernstorfer, V. S. Yakovlev, M. I. Stockman, and F. Krausz, "Optical-field-induced current in dielectrics," *Nature* **493**, 70 (2013).
10. M. Schultze, K. Ramasesha, C. Pemmaraju, S. Sato, D. Whitmore, A. Gandman, J. S. Prell, L. Borja, D. Prendergast, K. Yabana, D. M. Neumark, and S. R. Leone, "Attosecond band-gap dynamics in silicon," *Science* **346**, 1348–1352 (2014).
11. T. Higuchi, C. Heide, K. Ullmann, H. B. Weber, and P. Hommelhoff, "Light-field-driven currents in graphene," *Nature* **550**, 224 (2017).
12. M. Hentschel, R. Kienberger, C. Spielmann, G. A. Reider, N. Milosevic, T. Brabec, P. Corkum, U. Heinzmann, M. Drescher, and F. Krausz, "Attosecond metrology," *Nature* **414**, 509 (2001).
13. A. Baltuška, T. Udem, M. Uiberacker, M. Hentschel, E. Goulielmakis, C. Gohle, R. Holzwarth, V. Yakovlev, A. Scrinzi, T. W. Hänsch, and F. Krausz, "Attosecond control of electronic processes by intense light fields," *Nature* **421**, 611 (2003).
14. G. Sansone, E. Benedetti, F. Calegari, C. Vozzi, L. Avaldi, R. Flammini, L. Poletto, P. Villoresi, C. Altucci, R. Velotta, S. Stagira, S. De Silvestri, and M. Nisoli, "Isolated single-cycle attosecond pulses," *Science* **314**, 443–446 (2006).
15. L. Xu, C. Spielmann, A. Poppe, T. Brabec, F. Krausz, and T. Hänsch, "Route to phase control of ultrashort light pulses," *Opt. letters* **21**, 2008–2010 (1996).
16. H. R. Telle, G. Steinmeyer, A. Dunlop, J. Stenger, D. Sutter, and U. Keller, "Carrier-envelope offset phase control: A novel concept for absolute optical frequency measurement and ultrashort pulse generation," *Appl. Phys. B* **69**, 327–332 (1999).
17. J. Reichert, R. Holzwarth, T. Udem, and T. W. Haensch, "Measuring the frequency of light with mode-locked lasers," *Opt. communications* **172**, 59–68 (1999).
18. A. Apolonski, A. Poppe, G. Tempea, C. Spielmann, T. Udem, R. Holzwarth, T. W. Hänsch, and F. Krausz, "Controlling the phase evolution of few-cycle light pulses," *Phys. Rev. Lett.* **85**, 740 (2000).
19. M. Kakehata, H. Takada, Y. Kobayashi, K. Torizuka, Y. Fujihira, T. Homma, and H. Takahashi, "Single-shot measurement of carrier-envelope phase changes by spectral interferometry," *Opt. letters* **26**, 1436–1438 (2001).
20. B. E. Schmidt, A. D. Shiner, P. Lassonde, J.-C. Kieffer, P. B. Corkum, D. M. Villeneuve, and F. Légaré, "Cep stable 1.6 cycle laser pulses at 1.8 μm," *Opt. express* **19**, 6858–6864 (2011).
21. M. Kurucz, S. Tóth, R. Flender, L. Haizer, B. Kiss, B. Persielle, and E. Cormier, "Single-shot cep drift measurement at arbitrary repetition rate based on dispersive fourier transform," *Opt. express* **27**, 13387–13399 (2019).
22. J. Moses, S.-W. Huang, K.-H. Hong, O. Mücke, E. Falcão-Filho, A. Benedick, F. Ilday, A. Dergachev, J. Bolger, B. Eggleton, and F. X. Kartner, "Highly stable ultrabroadband mid-ir optical parametric chirped-pulse amplifier optimized for superfluorescence suppression," *Opt. letters* **34**, 1639–1641 (2009).
23. S.-W. Huang, G. Cirmi, J. Moses, K.-H. Hong, S. Bhardwaj, J. R. Birge, L.-J. Chen, E. Li, B. J. Eggleton, G. Cerullo, and F. X. Kartner, "High-energy pulse synthesis with sub-cycle waveform control for strong-field physics," *Nat. photonics* **5**, 475 (2011).
24. Y. Nomura, H. Shirai, and T. Fuji, "Frequency-resolved optical gating capable of carrier-envelope phase determination," *Nat. communications* **4**, 1–11 (2013).
25. Q. Wu and X.-C. Zhang, "Free-space electro-optic sampling of terahertz beams," *Appl. Phys. Lett.* **67**, 3523–3525 (1995).
26. S. Keiber, S. Sederberg, A. Schwarz, M. Trubetskov, V. Pervak, F. Krausz, and N. Karpowicz, "Electro-optic sampling of near-infrared waveforms," *Nat. Photonics* **10**, 159 (2016).
27. D. Sanchez, M. Hemmer, M. Baudisch, S. Cousin, K. Zawilski, P. Schunemann, O. Chalus, C. Simon-Boisson, and J. Biegert, "7 μm, ultrafast, sub-millijoule-level mid-infrared optical parametric chirped pulse amplifier pumped at 2 μm," *Optica* **3**, 147–150 (2016).
28. A. Leblanc, G. Dalla-Barba, P. Lassonde, A. Laramee, B. E. Schmidt, E. Cormier, H. Ibrahim, and F. Légaré, "High-field mid-infrared pulses derived from frequency domain optical parametric amplification," *Accept. to Opt. Lett. - https://doi.org/10.1364/OL.389804* (2020).
29. I. Pupeza, D. Sánchez, J. Zhang, N. Lilienfein, M. Seidel, N. Karpowicz, T. Paasch-Colberg, I. Znakovskaya, M. Pescher, W. Schweinberger *et al.*, "High-power sub-two-cycle mid-infrared pulses at 100 mhz repetition rate," *Nat. Photonics* **9**, 721 (2015).
30. C. Gaida, M. Gebhardt, T. Heuermann, F. Stutzki, C. Jauregui, J. Antonio-Lopez, A. Schülzgen, R. Amezcua-Correa, A. Tünnermann, I. Pupeza, and J. Limpert, "Watt-scale super-octave mid-infrared intrapulse difference frequency generation," *Light. Sci. & Appl.* **7**, 94 (2018).
31. T. Butler, D. Gerz, C. Hofer, J. Xu, C. Gaida, T. Heuermann, M. Gebhardt, L. Vamos, W. Schweinberger, J. Gessner *et al.*, "Watt-scale 50-mhz source of single-cycle waveform-stable pulses in the molecular fingerprint region," *Opt. letters* **44**, 1730–1733 (2019).
32. T. Butler, N. Lilienfein, J. Xu, N. Nagl, C. Hofer, D. Gerz, K. Mak, C. Gaida, T. Heuermann, M. Gebhardt *et al.*, "Multi-octave spanning, watt-level ultrafast mid-infrared source," *J. Physics: Photonics* **1**, 044006 (2019).
33. N. Ishii, K. Kaneshima, K. Kitano, T. Kanai, S. Watanabe, and J. Itatani, "Carrier-envelope phase-dependent high harmonic generation in the water window using few-cycle infrared pulses," *Nat. communications* **5**, 3331 (2014).

34. S. M. Teichmann, F. Silva, S. Cousin, M. Hemmer, and J. Biegert, "0.5-kev soft x-ray attosecond continua," *Nat. communications* **7**, 11493 (2016).
35. J. Li, X. Ren, Y. Yin, K. Zhao, A. Chew, Y. Cheng, E. Cunningham, Y. Wang, S. Hu, Y. Wu, M. Chini, and Z. Chang, "53-attosecond x-ray pulses reach the carbon k-edge," *Nat. communications* **8**, 186 (2017).
36. S. Ghimire, A. D. DiChiara, E. Sistrunk, P. Agostini, L. F. DiMauro, and D. A. Reis, "Observation of high-order harmonic generation in a bulk crystal," *Nat. physics* **7**, 138 (2011).
37. G. Vampa, T. Hammond, N. Thiré, B. Schmidt, F. Légaré, C. McDonald, T. Brabec, and P. Corkum, "Linking high harmonics from gases and solids," *Nature* **522**, 462 (2015).
38. M. Hohenleutner, F. Langer, O. Schubert, M. Knorr, U. Huttner, S. W. Koch, M. Kira, and R. Huber, "Real-time observation of interfering crystal electrons in high-harmonic generation," *Nature* **523**, 572–575 (2015).
39. U. Frühling, M. Wieland, M. Gensch, T. Gebert, B. Schütte, M. Krikunova, R. Kalms, F. Budzyn, O. Grimm, J. Rossbach, J. Plonjes, and M. Drescher, "Single-shot terahertz-field-driven x-ray streak camera," *Nat. Photonics* **3**, 523 (2009).
40. A. Baltuška, T. Fuji, and T. Kobayashi, "Controlling the carrier-envelope phase of ultrashort light pulses with optical parametric amplifiers," *Phys. review letters* **88**, 133901 (2002).
41. H. Liang, P. Krogen, Z. Wang, H. Park, T. Kroh, K. Zawilski, P. Schunemann, J. Moses, L. F. DiMauro, F. X. Kärtner, and K.-H. Hong, "High-energy mid-infrared sub-cycle pulse synthesis from a parametric amplifier," *Nat. communications* **8**, 141 (2017).
42. C. Manzoni, M. Först, H. Ehrke, and A. Cavalleri, "Single-shot detection and direct control of carrier phase drift of midinfrared pulses," *Opt. letters* **35**, 757–759 (2010).
43. Y. S. You, M. Wu, Y. Yin, A. Chew, X. Ren, S. Gholam-Mirzaei, D. A. Browne, M. Chini, Z. Chang, K. J. Schafer, M. B. Gaarde, and S. Ghimire, "Laser waveform control of extreme ultraviolet high harmonics from solids," *Opt. letters* **42**, 1816–1819 (2017).
44. Y. S. You, Y. Yin, Y. Wu, A. Chew, X. Ren, F. Zhuang, S. Gholam-Mirzaei, M. Chini, Z. Chang, and S. Ghimire, "High-harmonic generation in amorphous solids," *Nat. communications* **8**, 724 (2017).
45. X. Song, R. Zuo, S. Yang, P. Li, T. Meier, and W. Yang, "Attosecond temporal confinement of interband excitation by intraband motion," *Opt. Express* **27**, 2225–2234 (2019).
46. D. Franz, S. Kaassamani, D. Gauthier, R. Nicolas, M. Kholodtsova, L. Douillard, J.-T. Gomes, L. Lavoute, D. Gaponov, N. Ducros *et al.*, "All semiconductor enhanced high-harmonic generation from a single nanostructured cone," *Sci. reports* **9**, 1–7 (2019).
47. B. E. Schmidt, N. Thiré, M. Boivin, A. Laramée, F. Poitras, G. Lebrun, T. Ozaki, H. Ibrahim, and F. Légaré, "Frequency domain optical parametric amplification," *Nat. communications* **5**, 1–8 (2014).
48. G. Ernotte, P. Lassonde, F. Légaré, and B. Schmidt, "Frequency domain tailoring for intra-pulse frequency mixing," *Opt. express* **24**, 24225–24231 (2016).
49. A. Leblanc, P. Lassonde, S. Petit, J.-C. Delagnes, E. Haddad, G. Ernotte, M. Bionta, V. Gruson, B. Schmidt, H. Ibrahim *et al.*, "Phase-matching-free pulse retrieval based on transient absorption in solids," *Opt. express* **27**, 28998–29015 (2019).
50. C. Haworth, L. Chipperfield, J. Robinson, P. Knight, J. Marangos, and J. Tisch, "Half-cycle cutoffs in harmonic spectra and robust carrier-envelope phase retrieval," *Nat. Phys.* **3**, 52–57 (2007).
51. C. Li, E. Moon, H. Wang, H. Mashiko, C. M. Nakamura, J. Tackett, and Z. Chang, "Determining the phase-energy coupling coefficient in carrier-envelope phase measurements," *Opt. letters* **32**, 796–798 (2007).
52. C. Li, E. Moon, H. Mashiko, H. Wang, C. M. Nakamura, J. Tackett, and Z. Chang, "Mechanism of phase-energy coupling in f-to-2f interferometry," *Appl. optics* **48**, 1303–1307 (2009).